Article:
Freeman, F.S.H.B., Sharp, J., Xi, J. et al. (2019) Influence of solidification cell structure on the martensitic transformation in additively manufactured steels. Additive Manufacturing, 30. 100917. ISSN: 2214-7810

https://doi.org/10.1016/j.addma.2019.100917

Additive Manufacturing 30 (2019) 100917

Contents lists available at ScienceDirect

Additive Manufacturing

journal homepage: www.elsevier.com/locate/addma

Full Length Article

Influence of solidification cell structure on the martensitic transformation in additively manufactured steels

Felicity S.H.B. Freeman*, Jo Sharp, Jiawei Xi, Iain Todd

Department of Materials Science & Engineering, University of Sheffield, Sheffield, S1 3JD, UK

ARTICLE INFO

Keywords:
Martensitic phase transformation
Ultrafine grained microstructure
Thermodynamics
Rapid solidification
Powder bed fusion

ABSTRACT

A key feature when using martensitic steels is the proportion of retained austenite present in the final component. Martensitic steels manufactured by laser powder-bed fusion (LPBF) have been shown to have more retained austenite than when conventionally manufactured. The LPBF microstructure is characterised by small grains containing ultrafine solidification cells (< 1 μm). This study shows that the solidification cells can fully suppress thermal martensite. The retained austenite is highly metastable, and will readily transform to deformation martensite either in-build from thermal strain or post-build from deformation. This raises concerns around sample preparation methods causing incorrect phase quantification in LPBF-built martensitic steels.

1. Introduction

17-4 PH is a precipitation-hardened stainless steel, widely used in both additive and traditional manufacturing. Under conventional processing it is martensitic, but the laser powder-bed fusion (LPBF) literature reports a dual-phase structure of α'-martensite with a significant proportion of retained γ-austenite. Different studies have reported a wide variation in the relative phase fractions, even when using similar build parameters and build environments (Table 1).

Fig. 1 shows an example microstructure from LPBF-built 17–4 PH [5], which is representative of the hierarchical microstructure observed in many LPBF-built steels. The microstructure is characterised by small grains, generally between 10 μm–100 μm, each containing a forest of solidification cells. The solidification cells are elongated in the direction of growth, and typically range from 0.2 μm to 2 μm in diameter, depending on local solidification rates. The cells are separated by dense walls of geometrically-necessary dislocations, caused by adjacent cells having slightly different crystallographic orientations [6].

This definition of grains and solidification cells follows the approach outlined in [6], where the solidification cells are of the micron length scale, while grains (up to 200 microns) contain multiple solidification cells of the same growth direction. This hierarchical structure, with grains and cells of these characteristic length scales, is observed across a wide range of additively manufactured steels including 316 L [6,7], 17–4 PH [1,8], H13 [9] and M300 [10,11].

A number of the studies listed in Table 1 attribute the elevated level of retained austenite to the effect of a reduction in austenite grain size suppressing the thermally-induced martensite start temperature [12]. However, they do not explore whether the martensite present is thermally-induced or deformation-driven, and do not consider whether the controlling length scale in the suppression of thermal martensite is the grain size or the solidification cell size. The solidification cell size has been shown to be the controlling length scale in the mechanical performance of LPBF-built steels, specifically for yield strength [6].

Further, much of the literature on LPBF-built 17–4 PH reports quantitative phase analysis from samples which have undergone some degree of surface preparation. It has been shown that the retained austenite in additively manufactured 17-4 PH is highly metastable, and can transform to deformation martensite either as a result of in-situ thermal strain during the build [5,13] or as a result of post-build deformation (e.g. tensile testing, polishing) [4,14]. This places a level of uncertainty on the quantitative phase analysis summarised in Table 1, and suggests that the as-built austenite content may be higher than reported.

This study now considers whether the solidification cell size is the controlling length scale for the thermally-induced martensite start temperature, M_s, in additively manufactured steels and how this affects the likelihood of forming thermally-induced or deformation-driven martensite in the as-built state.

2. Experimental method

The 17–4 PH powder used was manufactured by EOS, in the 15 μm–45 μm size range, to the chemistry shown in Table 2 [5].

* Corresponding Author.
E-mail address: fshbf2@cantab.net (F.S.H.B. Freeman).

https://doi.org/10.1016/j.addma.2019.100917
Received 10 July 2019; Received in revised form 7 October 2019; Accepted 14 October 2019
Available online 24 October 2019

Table 1
Summary of quantitative phase analysis from LPBF-built samples of 17-4 PH.

	α (wt%)	γ (wt%)	Build Atmosphere	Power (W)	Speed (mm/s)	Layer (μm)	Hatch (μm)
[1]	25–50	50–75	Nitrogen	195	800	40	100
[2]	70–75	25–30	Nitrogen	195	600–1200	40	100
[2]	68–76	24–32	Nitrogen	70–195	287–800	40	100
[3]	15	85	Nitrogen	200	1000	20	100
[1]	92	8	Argon	195	800	40	100
[4]	28	72	Argon	200	*Data not provided*		
[5]	0–28	72–100	Argon	200	280–738	40	30–90
[3]	≈100	≈0	Argon	200	1000	20	100

The M300 (18-Ni300) powder was manufactured by LPW, now Carpenter Additive, again to a 15 μm–45 μm size range, to the chemistry shown in Table 3.

All samples were built on a Renishaw SLM125, using argon as the build environment. The build parameters are shown in Table 4, and the builds used a meander scan strategy with 67° rotation between layers. The samples were cylinders, 10 mm high and 8 mm diameter, and 10 mm cubes. After building the samples were removed from the baseplate by electro-discharge machining (EDM).

The 17-4 PH build did include samples with smaller point spacing and hatch spacing (higher energy density) than shown in Table 4, but these are not part of this analysis and results from them are discussed elsewhere [5,13]. Data from those samples is included in Fig. 3b and c, but the low energy density sample under consideration here, corresponding to the build parameters above, is circled.

Optical microscopy and scanning electron microscopy (SEM) were carried out on a mechanically sectioned surface from a cube of 17-4 PH. The surface was ground and polished, down to 1 μm diamond suspension, and etched with either Kallings #2 or 2% Nital. This surface preparation is expected to have caused deformation-driven phase transformation of retained austenite to martensite, but as this is a displacive transformation the physical arrangement and length scales of grains and solidification cells should be unaffected. The SEM images for 17-4 PH were taken using a FEI Nova 450 at the University of Sheffield, operating at 20 kV. The SEM images for M300 were taken using a FEI InspectF at the University of Sheffield, operating at 10 kV.

Vibrating sample magnetometer (VSM) data for 17-4 PH was generated from a 1.5 mm thick slice across the top of the cylinder, cut by EDM. The VSM was a MicroSense Model 10 at the University of Manchester. All measurements were carried out with the field perpendicular to the build direction. The measurement program and the method for converting the saturation magnetisation observed in VSM into a martensite phase fraction (in wt%) are covered in the Appendix. While the VSM output is information-rich (including saturation magnetisation, coercivity etc) it is restricted to small, thin samples (8 mm diameter, 2 mm thickness), is comparatively slow (1–2 hours per sample), and cannot easily be used to track martensitic transformation during mechanical or thermal processing.

Table 2
17-4 PH powder chemistry measured by AMG Analytical (wt%).

Fe	Cr	Ni	Cu	Mn	Si	Nb	C	Mo	Co	S	P
Bal	15.51	4.56	4.31	0.79	0.71	0.26	0.05	0.09	0.05	0.007	0.014

For 17-4 PH, Feritscope measurements were taken from slices EDM-cut from further down the cylinder samples. The Feritscope was a Fischer Feritscope MP30, and at least 4 measurements were taken on each sample to generate a mean and standard error. The Feritscope was calibrated in wt% using a set of standards purchased from Fischer, covering a range from 0.69 wt% to 84.4 wt%, so there was no requirement to convert between Ferrite number and wt%. Feritscope is only a surface measurement technique, but has the benefit of instant quantitative readings that can be taken during a trial and there is no restriction on sample size.

XRD was carried out on the EDM-cut surfaces previously used for Feritscope measurement, with no further surface preparation, using a PANalytical X'Pert3 Powder with Cu Kα radiation (not mono-chromated) at a step size of 0.0394° and a time per step of 1120s. Additional scans were carried out with a time per step of 5000 s.

EDM is judged to be a low deformation cutting technique when compared with mechanical sectioning. It is acknowledged that it causes some thermal processing, and results in the formation of a thin (5 μm–10 μm) recast layer [15]. This was observed in the XRD data as a face-centred cubic (FCC) peak at slightly lower 2θ than the bulk austenite peak, corresponding to a lattice parameter of $a = 3.64$ Å (Appendix Figure A8). This is consistent with the structure and lattice parameter expected from a compositional blend between the bulk 17-4 PH austenite (FCC, $a = 3.59$ Å [12,16,17]) and the Cu65:Zn35 brass wire (FCC, $a = 3.69$ Å [18]) used for cutting.

XRD is a surface measurement technique; 95% of the data is generated from the top 2 μm of material [19]. The XRD traces are therefore

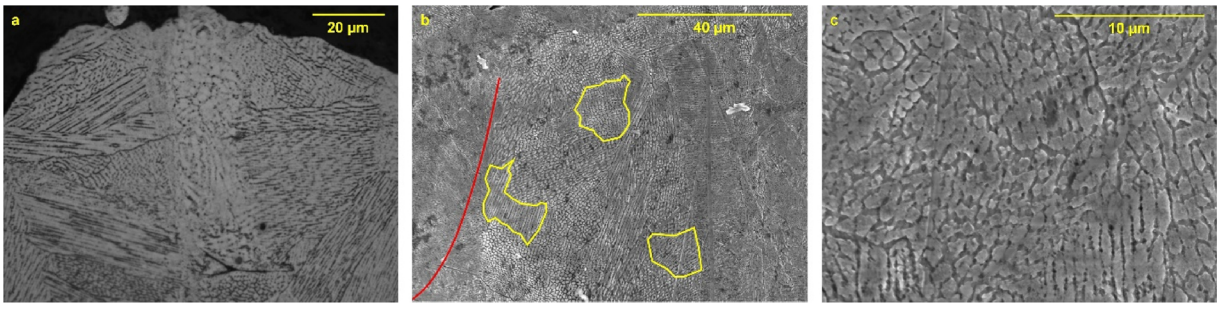

Fig. 1. A fully austenitic sample of LPBF-built 17-4 PH [5]. a) Optical image from top surface of sample, scale bar 20 μm; b) SEM image from bulk of sample, yellow lines indicate grain boundaries, red line indicates melt pool boundary, scale bar 40 μm; c) SEM image of solidification cells, scale bar 10 μm. The build direction is vertical in all images. Etched with Kallings #2 reagent. (For interpretation of the references to colour in this figure legend, the reader is referred to the web version of this article).

Table 3
M300 powder chemistry from Certificate of Conformity (wt%).

Fe	Ni	Co	Mo	Ti	Cr	Si	Mn	O	Al	N	C	S	P
Bal	17.91	9.2	4.8	1.1	0.13	0.04	0.02	0.02	0.1	< 0.01	< 0.01	0.002	< 0.005

Table 4
Renishaw SLM125 build parameters.

Power (W)	Exposure (μs)	Point (μm)	Speed (mm/s)	Layer (μm)	Hatch (μm)
200	100	90	738	40	90

far more strongly affected by the presence of the recast layer than the VSM measurements, which are taken from a bulk sample. Rietveld refinement was attempted on the XRD data, but it was not possible to get a repeatable convergence. This was attributed to the overlap between the peaks for the recast layer and the bulk austenite, and the inherent texture of additively manufactured materials. Instead the XRD data has been used for phase identification, and for comparative analysis between the same sample in different preparation conditions.

While Feritscope was used for quantitative phase analysis in the cooling trial, this was judged acceptable based on comparisons between Feritscope and VSM data, and the way the data was being used. There is more detail on this in the results section, where data from the cooling trial is presented.

The first cooling trial used methanol in a table-top laboratory chiller. The 17-4 PH sample was placed in the methanol bath, and progressively cooled to −37 °C. Measurements of wt% martensite were taken by Feritscope before and during the cooling process, sampling four different measurement locations at each temperature.

The second trial submerged the sample in liquid nitrogen for at least 1 h. For 17-4 PH, twelve measurements of wt% martensite were taken by Feritscope at room temperature before cooling, and again when the sample returned to room temperature after cooling. The sample then measured by XRD after it had returned to room temperature. For M300 the sample was measured by XRD before and after cooling in liquid nitrogen.

For 17-4 PH the cooling trials were carried out on 1 mm thick slices, EDM-cut parallel to the baseplate from a 10 mm cube. For M300 they were carried out on half-cylinders, made by EDM-cutting along the cylinder axis. Both of these were judged to have sufficiently small thermal mass to experience high cooling rates and reach equilibrium quickly when submerged in liquid nitrogen from room temperature.

3. Prediction of M_s in 17-4 PH

The effect of austenite grain size on martensite start temperature, M_s, is well known, and has been observed in a range of alloys [12,20,21]. A relationship between grain size and M_s has been established for a range of steel compositions, validated for grain sizes in the range 1 μm–500 μm (Eq. 1) [12]. In this, $f = 0.01$ is the first detectable fraction of martensite, $m = 0.05$ is the martensite plate aspect ratio and V_γ is the volume of the austenite grain in μm^3.

$$M_s^0 - M_s = \frac{1}{0.253}\ln\left[\frac{1}{1.57\times10^{-21}V_\gamma}\left\{\exp\left(-\frac{\ln(1-f)}{m}\right)-1\right\}+1\right] \quad (1)$$

This is based on geometric partitioning analysis describing the relationship between the number of martensite plates per unit volume, the fraction of martensite, the aspect ratio of the martensite plates and the size of austenite compartments after being split by a martensite plate. This was combined with experimental data for the number of martensite plates per unit volume as a function of temperature, and the fitting constants were determined from data on M_s as a function of grain size for a range of alloys. The overall relationship is therefore theoretically determined, and only the fitting constants are experimentally determined. The alloys used in the experimental data cover a wide range of both low-alloy and more richly alloyed steels. Their composition range covers that of 17-4 PH, except for chromium and copper.

Eq. 1 uses a theoretical large-grain martensite start temperature, M_s^0, which is defined as the point when martensite becomes thermodynamically possible; when the free energy change $\nabla G^{\gamma\alpha}$ from austenite to ferrite of the same composition is sufficient to provide the driving force for nucleation. This critical value, $\nabla G_C^{\gamma\alpha}$, is itself composition dependent.

An expression has been published for calculating $\nabla G^{\gamma\alpha}$ from the atomic fraction X_i of each element in the alloy (Eq. 2), but this was established at an experimentally determined M_s, so will itself have been influenced by the grain size of the samples [22,23].

$$\begin{aligned}\Delta G^{\gamma\alpha} = {} & 1010 + 4009X_C^{0.5} + 1879X_{Si}^{0.5} + 1980X_{Mn}^{0.5} + 172X_{Ni}^{0.5} + 1418X_{Mo}^{0.5} \\ & + 1868X_{Cr}^{0.5} + 1618X_V^{0.5} + 752X_{Cu}^{0.5} + 714X_W^{0.5} + 1653X_{Nb}^{0.5} \\ & + 3097X_N^{0.5} - 352X_{Co}^{0.5}\end{aligned} \quad (2)$$

Instead, the M_s reported for a sample of 17-4 PH with a known grain size and chemistry was used to calculate M_s^0, with adjustments to account for the minor compositional differences between that sample and the alloy used in this study [24]. This is covered in detail in the Appendix.

This composition-specific M_s^0 was used to predict the relationship between austenite grain size, L_γ, and martensite start temperature for the exact composition of 17-4 PH used (Fig. 2 a). This relationship was

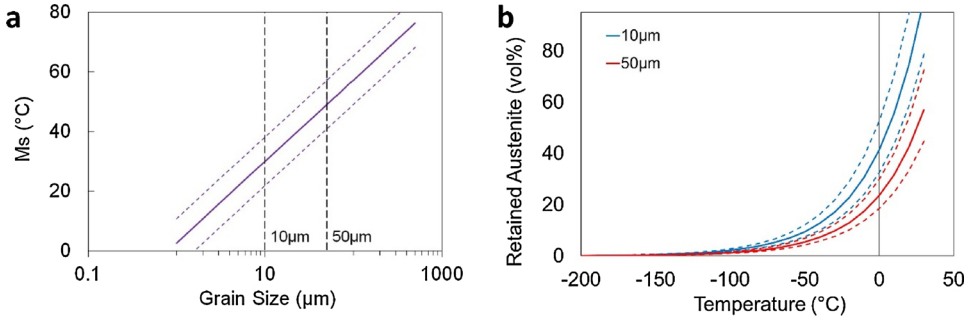

Fig. 2. a) Prediction of M_s as a function of austenite grain size; b) Predicted retained austenite volume fraction as a function of temperature for 10 μm and 50 μm austenite grain sizes. In both cases, dotted lines indicate prediction error, see Appendix for details.

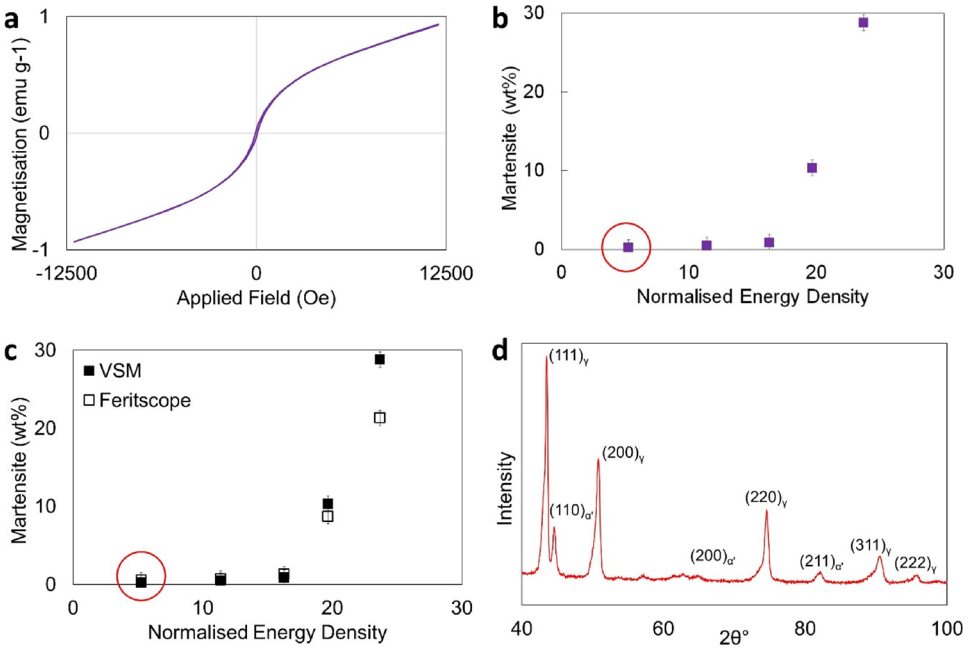

Fig. 3. a) VSM data for 17-4 PH sample showing majority paramagnetic (austenite) contribution with only small ferromagnetic (martensite) contribution [5]; b) Martensite wt % in 17-4 PH determined from VSM saturation magnetisation against build energy density; c) Comparison of VSM and Feritscope data from 17-4 PH showing good agreement when martensite phase fraction < 10 wt%, error bars show standard error across repeat Feritscope measurements [13]; d) XRD data from 17-4 PH sample showing majority austenite and minority martensite, generated at 1120s per step.

calculated for the range 1 µm–500 µm, corresponding to the range over which Eq. 1 was shown to be valid [12]. The prediction error is generated from a combination of error in grain size measurement from [24].

This shows a predicted M_s for large grained material (1000 µm) much lower than that which might be expected, up to only 80 °C compared with the quoted values for 17-4 PH of 105 °C–132 °C [24–26]. This shift is primarily due to the composition of the powder being considered. The alloy used here (Table 2) had more silicon and nitrogen than was reported for the comparison alloy [24]. This resulted in an increased value of $\Delta G^{\gamma\alpha}$ as well as a shift in the free energy curves for austenite and ferrite.

The predicted M_s was combined with the Koistinen-Marburger relationship (Eq. 3) to predict the volume fraction of retained austenite at room temperature, T_{RT}, as a function of austenite grain size (Fig. 2b) [26]. The fitting constant $\alpha = 0.02955$ is taken from a fit to neutron diffraction data from 17-4 PH on cooling [24].

$$f_\gamma = \exp(\alpha \{M_s - T_{RT}\}) \quad (3)$$

While this calculates the volume fraction, given that the volume expansion on transformation from austenite to martensite is only ~3%, this has been taken to be equivalent to weight fraction for this analysis.

From the prediction above, grain sizes in the range 10 µm–50 µm, at the lower end of the characteristic range, would be expected to suppress M_s to 30 °C–50 °C, giving 40 vol%-70 vol% retained austenite at room temperature. This is a conservative approach; if the M_s were higher than this prediction, closer to the values reported in literature, then the expected phase fraction martensite for a given grain size would be higher.

Comparing this with the data in Table 1, the values appear roughly consistent with suppression by the grain size, at a controlling length scale of 10 µm–50 µm. The main discrepancy is the fully austenitic structure reported in [5], which would suggest a controlling length scale closer to that of the solidification cells.

All of the studies in Table 1, with the exception of [5], report quantitative phase analysis (QPA) measured only from XRD traces and the majority state that the sample had been mechanically prepared before measurement (cut, ground, polished). In contrast, the analysis in [5] used XRD for phase identification, but then based the quantitative phase analysis on VSM, a bulk technique which would be less affected by any surface transformation. These results are summarised in Fig. 3, with the sample under consideration in this study circled in Fig. 3b-c.

It has been shown that metastable retained austenite in LPBF-built 17-4 PH can transform to deformation martensite [4,5,14]. It is suggested that, for the other samples listed in Table 1, this could have occurred during the sample preparation, and the fraction austenite in the as-built state could have been higher than reported.

This would explain the wide range in reported phase fraction austenite, from samples with similar build conditions, and explain why a fully austenitic structure was reported in [5] when all other studies have reported some martensite. Therefore, the apparent correlation between the reported austenite content in Table 1 and the prediction in Fig. 2 is not sufficient to confirm that the grain size is the controlling length scale.

4. Results

Reviewing Fig. 2, if the grain size is the controlling length scale, then it would be expected that cooling to -30 °C would result in 80 vol %-90 vol% thermal martensite. Cooling in liquid nitrogen (−196 °C) would give > 99 vol% thermal martensite. To test this, samples of the LPBF-built 17-4 PH material were cooled to −37 °C in methanol and to −196 °C in liquid nitrogen.

In both cases measurements were taken by Feritscope on a surface cut by EDM. While Feritscope is a surface method, and therefore will be affected by the recast layer, the measurements are for comparative analysis, looking for a change in the martensite content as a result of the cooling process.

Data presented above (Fig. 3c) shows that Feritscope (surface) and VSM (bulk) measurements from an EDM-cut surface are in good agreement for low martensite contents, although they diverge at higher martensite contents, with Feritscope generally measuring lower than VSM, presumably due to the recast layer. However, if grain size is the controlling length scale, then sub-zero cooling would be expected to result in > 50 wt% martensite. The data in Fig. 3c gives confidence that this would register in the Feritscope reading, even if VSM were then required to measure a more accurate phase fraction.

In summary, the use of Feritscope in this trial is judged acceptable due to the comparative nature of the analysis, combined with the expected magnitude of the martensite phase fraction if grain size were the controlling length scale.

Before cooling both samples showed an initial level of (0.38 ± 0.01) wt% martensite; the martensite present was attributed

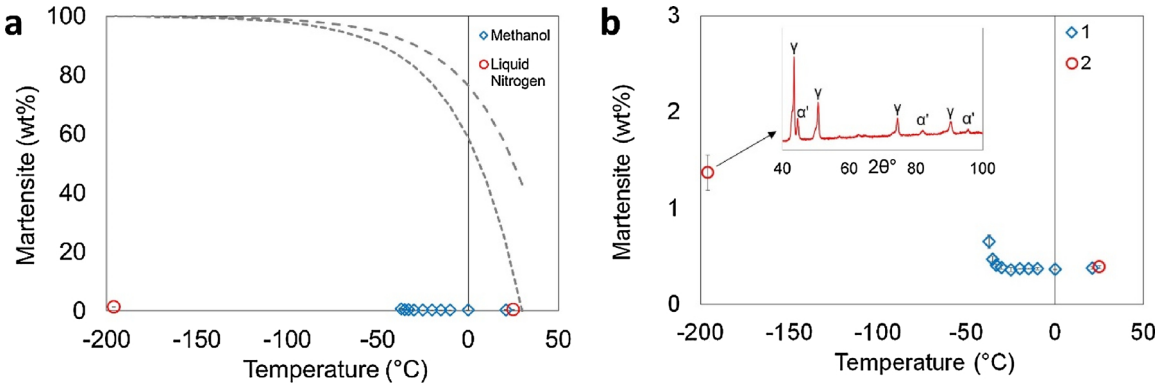

Fig. 4. a) Effect of sub-zero cooling on martensite phase fraction in LPBF-built 17-4 PH, blue diamonds: Sample 1, martensite wt% on cooling to −37 °C in methanol, red circles: Sample 2, martensite wt% on cooling to −196 °C in liquid nitrogen, grey lines: predicted martensite wt% for 10 µm and 50 µm austenite grain size (from Fig. 2d); b) As (a) but with expanded scale and insert showing XRD trace for Sample 2 after cooling. Error bars show standard error. (For interpretation of the references to colour in this figure legend, the reader is referred to the web version of this article).

to deformation-driven transformation triggered by EDM when removing the sample from the baseplate and cutting the slice. Sample 1 showed no further transformation on cooling to 0 °C. There was a very slight increase in martensite content on cooling from −30 °C to −37 °C, up to (0.66 ± 0.07) wt%, although this was accompanied by an increase in the standard error and may be within the measurement error of the Feritscope. Sample 2 showed similar behaviour with a very slight increase in martensite content, up to (1.37 ± 0.18) wt% after 3 h at −196 °C.

While both samples showed some martensitic transformation, the extent was much smaller than the > 80 vol% martensite expected from grain size limited transformation (Fig. 4a). The XRD trace (Fig. 4b insert) confirmed the Feritscope result, showing small peaks for martensite and strong peaks for austenite. As explained earlier, it was not possible to achieve a good quality Rietveld refinement on the XRD data for quantitative phase analysis.

To confirm this result, a similar trial was carried out on M300, also known as 18-Ni300. This has a higher martensite start temperature (280 °C [27]), so would be expected to have a higher proportion of martensite at room temperature for the same grain size. The literature on LPBF processed M300 shows that it has the same characteristic hierarchical microstructure as illustrated above, and on the same length scale [10,28]. In the as-built condition, the phase fraction of martensite has been reported to vary between 88.6 % [10] and 94.2 % [28], although this was again from samples which had undergone some surface preparation before XRD.

Initially, the as-built surface was measured by Feritscope in three separate locations, with three repeats in each location. This gave a reading of (50.2 ± 1.5) wt% martensite, which is considerably lower than that reported in literature [10,28]. The measurement variation is comparatively high, due to measuring on the rough, as-built surface but this avoided any influence from the recast layer on an EDM-cut face. This cannot distinguish between thermally-induced martensite which had transformed on cooling, or deformation-martensite resulting from in-situ thermal strain during the build.

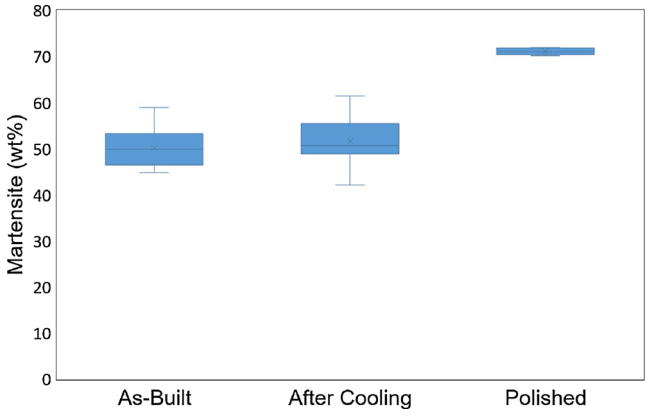

Fig. 5. Effect of sub-zero cooling and surface polishing on martensite phase fraction in LPBF-built M300.

If the martensite was thermally-induced, then further cooling would be expected to drive further transformation, in accordance with the Koistinen-Marburger relationship (Eq. 3). The sample was cooled in liquid nitrogen for 2 h, returned to room temperature and the measurement was repeated, giving a reading of (51.7 ± 1.8) wt% martensite (Fig. 5). This is within the error from the previous measurement, indicating that there had been no further transformation.

To test the susceptibility to deformation-driven transformation, the same sample was then subjected to very gentle polishing with P2500 grit paper, which would be expected to cause some local surface deformation. After polishing, the sample was re-measured and the Feritscope reading had now increased to (71.1 ± 0.2) wt% martensite. This was a significant increase, indicating considerable deformation-driven transformation had occurred. The reduction in error is due to the reduced roughness in the measurement surface.

Optical microscopy of the M300 sample showed clear keyhole melt pools, approximately 100 µm–150 µm in depth and 100 µm in width (Fig. 6a). At higher magnification it could be seen that these contained the expected hierarchical microstructure, with grains ranging from 10 µm to 100 µm in length, containing extremely fine solidification cells (Fig. 6b-c & Appendix Figure A10). These were generally between 0.3 µm and 1.3 µm across (Figure A11). This is consistent with the microstructure reported elsewhere for LPBF-build M300 [10,11].

5. Discussion

In this work, it is shown that 17-4 PH and M300 produced by LBPF have comparable microstructures, with micron-scale solidification cells, and both show complete suppression of thermally-induced martensitic transformation, even on cooling in liquid nitrogen (−196 °C). Both also show a deformation-driven transformation in response to either in-situ or post-build deformation.

If the grain size were the controlling length scale for the thermally-induced transformation mechanism, then both materials would be expected to show transformation when cooled in liquid nitrogen. While the prediction of M_s for 17-4 PH shown in Fig. 2 cannot necessarily be extrapolated to length scales below 1 µm, it does suggest that the controlling length scale must be of this order of magnitude to get the observed level of thermal martensite suppression. For M300 the

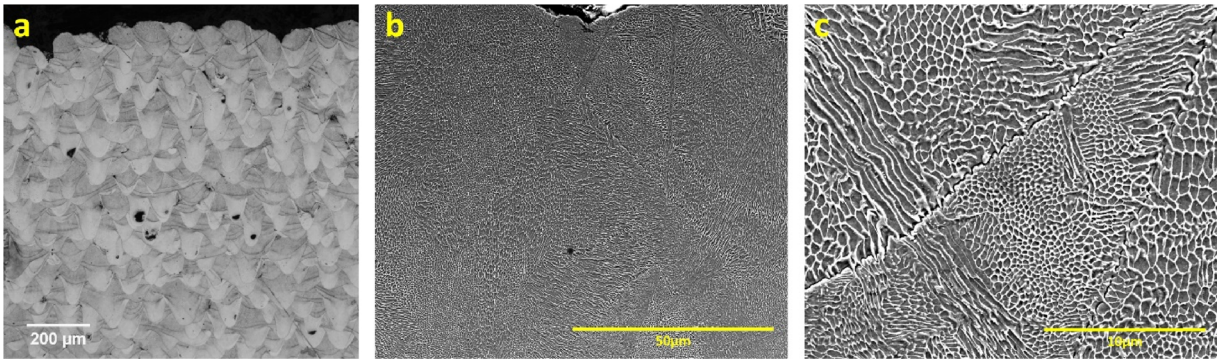

Fig. 6. Microscopy of M300 sample. a) Optical overview including build surface and bulk material with keyhole melt pools (200 µm scale bar); b) SEM of surface showing cellular structure (50 µm scale bar); c) SEM of bulk material showing cellular structure (10 µm scale bar). The build direction is vertical in all images. Etched with 2% Nital.

martensite start temperature should be higher, making it even less likely that full suppression could be achieved with grain size as the controlling length scale.

Complete suppression of thermally-induced martensitic transformation has been reported elsewhere for material with an austenite grain size of 0.8 µm [20], which is comparable with the solidification cell size. It was shown that, in these ultra-fine grains, the strain energy associated with multi-variant nucleation was extremely high and therefore very unlikely, but that single variant transformation required an unachievable level of undercooling. The result was that thermally driven martensitic transformation was fully suppressed, even after cooling in liquid nitrogen.

The importance of solidification cell size on mechanical behaviour of LPBF-built materials has been demonstrated elsewhere [6]. This showed that, while the misorientation between the cells was comparatively low at only 1-2° [6,29], under tensile testing, the dense dislocation walls around the solidification cells were sufficiently robust to strengthen the material in a manner normally attributed to grain boundaries. Further, it was shown in [6] that there was a strong dislocation trapping and retention mechanism inside the cell walls.

In this study, it is suggested the solidification cells are the controlling length scale for thermally-induced martensite; the dense dislocation walls being sufficiently robust to prevent the displacive martensitic transformation crossing them. If the dense dislocation walls were not able to prevent martensite growth, then the controlling length scale would be the grain size, and there would be thermally-induced transformation on cooling to −196 °C. As this did not happen, the conclusion is that the controlling length scale is the solidification cell size, and that the dense dislocation walls must be sufficiently robust to stop thermal martensite.

The microscopy of both 17-4 PH (Fig. 1) and M300 (Fig. 6) samples show that the solidification cell size is not completely uniform across the material; it will vary depending on the local solidification conditions. Eq. 4 is an empirical relationship between the cooling rate $\dot{T}$ and primary dendrite arm spacing λ_1 (solidification cell diameter), where a and n are material dependent constants, determined to be a = 60–100 ms/K and n = 0.2-0.5 for steels [30–32].

$$\lambda_1 = a\,\dot{T}^{-n} \tag{4}$$

Using Eq. 4, an increase in cooling rate from 10^5 K/s to 10^7 K/s would result in a comparatively small change in solidification cell size, from 1.4 µm to 0.3 µm. This indicates how characteristic the micron length scale is for solidification cells in LPBF-built steels, across a wide range of processing conditions and positions within the melt pool.

The very low level of martensitic transformation seen in the 17-4 PH sample after cooling below 0 °C (Fig. 4) may be due to limited thermally-induced martensitic transformation taking place in the larger solidification cells, or where the cell walls are slightly less heavily dislocated.

6. Conclusions

A hierarchical microstructure is characteristic of LPBF-built steels, with grains of 10 µm–100 µm containing solidification cells of 0.2 µm–2 µm, which are surrounded by dense dislocation walls. These walls have been shown to have a mechanical strengthening effect comparable with grain boundaries.

It has been previously shown that it is possible to achieve a fully austenitic structure in LPBF-built 17-4 PH. Here, it has been demonstrated that this is stable on cooling in liquid nitrogen, with no thermally-induced martensitic transformation. Similar results were observed in M300, with 50 wt% martensite in the as-built condition, but no further transformation on cooling in liquid nitrogen. This indicates that, in both materials, the thermally-induced transformation mechanism has been suppressed.

Suppression of thermally-induced martensite to this extent is not consistent with the grain size being the controlling length scale. It is therefore concluded that the solidification cell size is the controlling length scale for thermally-induced martensite in LPBF of martensitic steels, and can actually suppress thermally-induced martensite completely. This results in an elevated level of retained austenite, which will readily transform to deformation martensite as a result of either in-situ thermal strain or post-build processing (e.g. grit-blasting, machining, sample preparation).

To get accurate phase quantification, it is essential to minimise, or at least understand the effect of, any post-build deformation or surface treatments. It may be more appropriate to use bulk measurement techniques (e.g. VSM), measure in the as-built condition without any surface preparation or use low-deformation techniques such as electro-polishing.

Much of the literature on LPBF-built martensitic steels reports phase fractions from ground and polished samples, where sample preparation may have caused the surface to transform, leading to a higher martensite content being reported. This should be taken into account when comparing the reported microstructure and mechanical properties. On a more positive note, this also suggests a method for achieving a spatially varied microstructure using LPBF to build a majority austenitic component, and then mechanically processing the surface to achieve a harder martensitic outer casing.

Funding

This work was supported by the Engineering and Physical Sciences Research Council in part by award reference 1686001 and in part by the Future Manufacturing Hub in Manufacture using Advanced Powder Processes (MAPP) (EP/P006566/1).

Contributions

FF carried out the builds in 17-4 PH and M300, and the XRD and

Feritscope analysis. JS and FF carried out the methanol and liquid nitrogen trials. JX and FF carried out the microscopy on M300. FF, JX, JS and IT analysed the data and developed the concept. FF wrote the manuscript. All authors reviewed the manuscript.

Declaration of Competing Interest

None.

Appendix A. Supplementary data

Supplementary material related to this article can be found, in the online version, at doi:https://doi.org/10.1016/j.addma.2019.100917.

References

[1] H.K. Rafi, D. Pal, N. Patil, T.L. Starr, B.E. Stucker, Microstructure and mechanical behavior of 17-4 precipitation hardenable steel processed by selective laser melting, J. Mater. Eng. Perform. 23 (2014) 4421–4428, https://doi.org/10.1007/s11665-014-1226-y.

[2] H. Gu, H. Gong, D. Pal, K. Rafi, T. Starr, B. Stucker, Influences of energy density on porosity and microstructure of selective laser melted 17-4PH stainless steel, Solid Freeform Fabr. Symp. Proc. (2013) 474–479, https://doi.org/10.1007/s13398-014-0173-7.2.

[3] L.E. Murr, E. Martinez, J. Hernandez, S. Collins, K.N. Amato, S.M. Gaytan, P.W. Shindo, Microstructures and properties of 17-4 PH stainless steel fabricated by selective laser melting, J. Mater. Res. Technol. 1 (2012) 167–177, https://doi.org/10.1016/S2238-7854(12)70029-7.

[4] L. Facchini, N. Vicente, I. Lonardelli, E. Magalini, P. Robotti, M. Alberto, Metastable austenite in 17-4 precipitation-hardening stainless steel produced by selective laser melting, Adv. Eng. Mater. 12 (2010) 184–188, https://doi.org/10.1002/adem.200900259.

[5] F.S.H.B. Freeman, A. Lincoln, J. Sharp, A. Lambourne, I. Todd, Exploiting thermal strain to achieve an in-situ magnetically graded material, Mater. Des. 161 (2019) 14–21, https://doi.org/10.1016/j.matdes.2018.11.011.

[6] Y.M. Wang, T. Voisin, J.T. Mckeown, J. Ye, N.P. Calta, Z. Li, Z. Zeng, Y. Zhang, W. Chen, T.T. Roehling, R.T. Ott, M.K. Santala, P.J. Depond, M.J. Matthews, A.V. Hamza, T. Zhu, Additively manufactured hierarchical stainless steels with high strength and ductility, Nat. Mater. 17 (2018) 63–70, https://doi.org/10.1038/NMAT5021.

[7] K. Saeidi, X. Gao, F. Lofaj, L. Kvetková, Z.J. Shen, Transformation of austenite to duplex austenite-ferrite assembly in annealed stainless steel 316L consolidated by laser melting, J. Alloys. Compd. 633 (2015) 463–469, https://doi.org/10.1016/j.jallcom.2015.01.249.

[8] S. Cheruvathur, E.A. Lass, C.E. Campbell, Additive manufacturing of 17-4 PH stainless steel: post-processing heat treatment to achieve uniform reproducible microstructure, JOM. 68 (2016) 930–942, https://doi.org/10.1007/s11837-015-1754-4.

[9] R. Mertens, B. Vrancken, N. Holmstock, Y. Kinds, J.-P. Kruth, J. Van Humbeeck, Influence of powder bed preheating on microstructure and mechanical properties of H13 tool steel SLM parts, Phys. Procedia 83 (2016) 882–890, https://doi.org/10.1016/j.phpro.2016.08.092.

[10] R. Casati, J. Lemke, A. Tuissi, M. Vedani, Aging behaviour and mechanical performance of 18-Ni 300 steel processed by selective laser melting, Metals (Basel). 6 (2016) 218, https://doi.org/10.3390/met6090218.

[11] E.A. Jägle, P.-P. Choi, J. Van Humbeeck, D. Raabe, Precipitation and austenite reversion behavior of a maraging steel produced by selective laser melting, J. Mater. Res. 29 (2014) 2072–2079, https://doi.org/10.1557/jmr.2014.204.

[12] H.-S. Yang, H.K.D.H. Bhadeshia, Austenite grain size and the martensite–start temperature, Scr. Mater. 60 (2009) 493–495, https://doi.org/10.1016/j.scriptamat.2008.11.043.

[13] F. Freeman, Structuring Difference: The Additive Manufacture of Spatially & Functionally Differentiated Microstructures, University of Sheffield, 2018 (Accessed September 3, 2019), http://etheses.whiterose.ac.uk/22742/.

[14] W.E. Luecke, J.A. Slotwinski, Mechanical properties of austenitic stainless steel made by additive manufacturing, J. Res. Inst. Stand. Technol. 119 (2014) 398–418, https://doi.org/10.6028/jres.119.015.

[15] T.R. Newton, S.N. Melkote, T.R. Watkins, R.M. Trejo, L. Reister, Investigation of the effect of process parameters on the formation and characteristics of recast layer in wire-EDM of Inconel 718, Mater. Sci. Eng. A. 513–514 (2009) 208–215, https://doi.org/10.1016/J.MSEA.2009.01.061.

[16] D.J. Dyson, B. Holmes, Effect of alloying additions on the lattice parameter of austenite, J. Iron Steel Inst. 208 (1970) 469–473.

[17] S.S. Babu, E.D. Specht, S.A. David, E. Karapetrova, P. Zschack, M. Peet, H.K.D.H. Bhadeshia, In-situ observations of lattice parameter fluctuations in austenite and transformation to bainite, Metall. Mater. Trans. A. 36A (2005) 3281–3289, https://doi.org/10.1007/s11661-005-0002-x.

[18] H.M. Otte, Lattice parameter studies of annealed, of aged, and of Cold-Worked Alpha Brass, J. Appl. Phys. 33 (1962) 1436–1441, https://doi.org/10.1063/1.1728750.

[19] B.D. Cullity, J.W. Weymouth, Elements of X-Ray diffraction, Am. J. Phys. 25 (1957) 394–395, https://doi.org/10.1119/1.1934486.

[20] S. Takaki, K. Fukunaga, J. Syarif, T. Tsuchiyama, Effect of grain refinement on thermal stability of metastable austenitic steel, Mater. Trans. 45 (2004) 2245–2251, https://doi.org/10.2320/matertrans.45.2245.

[21] J.R.C. Guimarães, P.R. Rios, The mechanical-induced martensite transformation in Fe-Ni-C alloys, Acta Mater. 84 (2015) 436–442, https://doi.org/10.1016/j.actamat.2014.10.040.

[22] T. Cool, H.K.D.H. Bhadeshia, Prediction of martensite start temperature of power plant steels, Mater. Sci. Technol. ISSN. 12 (1996) 40–44, https://doi.org/10.1179/mst.1996.12.1.40.

[23] G. Ghosh, G.B. Olson, Kinetics of FCC→ BCC heterogeneous martensitic nucleation—I. The critical driving force for athermal nucleation, Acta Metall. Mater. 42 (1994) 3361–3370, https://doi.org/10.1016/0956-7151(94)90468-5.

[24] F. Christien, M.T.F. Telling, K.S. Knight, A comparison of dilatometry and in-situ neutron diffraction in tracking bulk phase transformations in a martensitic stainless steel, Mater. Charact. 82 (2013) 50–57, https://doi.org/10.1016/j.matchar.2013.05.002.

[25] C.N. Hsiao, C.S. Chiou, J.R. Yang, Aging reactions in a 17-4 PH stainless steel, Mater. Chem. Phys. 74 (2002) 134–142, https://doi.org/10.1016/S0254-0584(01)00460-6.

[26] D.P. Koistinen, R.E. Marburger, A general equation prescribing the extent of the austenite-martensite transformation in pure iron-carbon alloys and plain carbon steels*, Acta Metall. 7 (1959) 59–60, https://doi.org/10.1016/0001-6160(59)90170-1.

[27] S.A. Khan, H.K.D.H. Bhadeshia, Kinetics of martensitic transformation in partially bainitic 300M steel, Mater. Sci. Eng. A. 129 (1990) 257–272, https://doi.org/10.1016/0921-5093(90)90273-6.

[28] K. Kempen, E. Yasa, L. Thijs, J.-P. Kruth, J. van Humbeeck, Microstructure and mechanical properties of Selective Laser Melted 18Ni-300 steel, Phys. Procedia 12 (2011) 255–263, https://doi.org/10.1016/j.phpro.2011.03.033.

[29] V.D. Divya, R. Muñoz-Moreno, O.M. Messé, J.S. Barnard, S. Baker, T. Illston, H.J. Stone, Microstructure of selective laser melted CM247LC nickel-based superalloy and its evolution through heat treatment, Mater. Charact. 114 (2016) 62–74, https://doi.org/10.1016/j.matchar.2016.02.004.

[30] I. Gilath, J.M. Signamarcheix, P. Bensussan, A comparison of methods for estimating the weld-metal cooling rate in laser welds, J. Mater. Sci. 29 (1994) 3358–3362, https://doi.org/10.1007/BF00356685.

[31] M. El-Bealy, B.G. Thomas, Prediction of dendrite arm spacing for low alloy steel casting processes, Metall. Mater. Trans. B. 27 (1996) 689–693, https://doi.org/10.1007/BF02915668.

[32] H. Jacobi, K. Schwerdtfeger, Dendrite morphology of steady state unidirectionally solidified steel, Metall. Trans. A. 7 (1976) 811–820, https://doi.org/10.1007/BF02644078.